# Metamaterial-based lossy anisotropic epsilon-near-zero medium for energy collimation

Nian-Hai Shen, Peng Zhang, Thomas Koschny, and Costas M. Soukoulis

Phys. Rev. B **93**, 245118 — Published 8 June 2016

DOI: 10.1103/PhysRevB.93.245118

# Exploration of metamaterial-based lossy anisotropic epsilon-near-zero medium for energy collimation

Nian-Hai Shen,[1,*] Peng Zhang,[1] Thomas Koschny,[1] and Costas M. Soukoulis[1,2]

[1] *Ames Laboratory—U.S. DOE and Department of Physics and Astronomy, Iowa State University, Ames, Iowa 50011, USA*
[2] *Institute of Electronic Structure and Laser, FORTH, 71110 Heraklion, Crete, Greece*

Lossy anisotropic epsilon-near-zero (ENZ) medium may lead to a counter-intuitive phenomenon of omnidirectional total refraction [S. Feng, Phys. Rev. Lett. **108**, 193904 (2012)], which offers a fabulous strategy for energy collimation and energy harvesting. Here, in the scope of effective medium theory, we systematically investigate two simple metamaterial configurations, i.e., metal-dielectric-layered structure and wire medium, to explore the possibility of fulfilling the conditions of such anisotropic lossy ENZ medium by playing with materials parameters. Both realistic metamaterial structures and their effective medium equivalences have been numerically simulated, and the results are in excellent consistency with each other. Our study provides a clear guidance and therefore paves the way towards the seek of proper designs of anisotropic metamaterials for a decent effect of energy collimation and wavefront manipulation.

## I. INTRODUCTION

Metamaterials with building blocks artificially structured at a subwavelength scale, have been a paradigm for manipulating propagation of waves and engineering electromagnetic space.[1–4] Besides the most well-known negative refraction,[5,6] super-resolution imaging,[7–10] optical cloaking[11–14] and metasurfaces,[15–17] the powerful concept of metamaterials also boosted the realization of zero-index medium[18–20] [$\varepsilon$-near-zero (ENZ) or $\mu$-near-zero (MNZ) or both], which leads to many fascinating properties including directive emission,[21,22] light squeezing,[23,24] scattering manipulation,[25–28] etc. Generally, intrinsic loss is a hinder in metamaterials,[1,29] which limits and challenges most of proposed applications, and thus gain-assisted metamaterials were raised and attracted extensive studies.[30–32] The only exception previously found with respect to the loss in metamaterials is perfect absorber, where loss is favored.[33] Recently, Feng revealed a counterintuitive phenomenon, i.e., so-called anti-Snell's law, with a loss-assisted anisotropic ENZ medium, where loss plays a positive role as well.[34] Such conceptual lossy anisotropic materials were proposed to have important applications in beam collimation and energy harvesting, a different strategy compared to some previous studied lossless or low-loss extremely anisotropic materials.[35–39] Even though there have been several metamaterial structures tested numerically[40] and experimentally[41] for the loss-induced transmission enhancement, so far it still lacks a clear guidance on practical constructions for such lossy anisotropic materials. In the current work, we systematically explore the possibilities of fulfilling the conditions of lossy anisotropic ENZ medium, by means of two simple metamaterial structures, i.e., metal-dielectric-layered stack and wire medium, respectively. We successfully demonstrate the effect of beam collimation with our practical designs, and our investigation enlightens the search of proper materials to the building of lossy anisotropic ENZ metamaterial structures or devices for beam steering and energy harvesting.

## II. RESULTS AND DISCUSSIONS

Firstly, we would like to revisit such a special category of lossy anisotropic materials in the way of equi-frequency contour (EFC). For simplicity, we can take non-magnetic materials under consideration in the present work and the corresponding permittivity tensor $\bar{\bar{\varepsilon}}$ is expressed in the following form under the principal coordinate system $(x, y, z)$:

$$\bar{\bar{\varepsilon}} = \begin{bmatrix} \varepsilon_x & 0 & 0 \\ 0 & \varepsilon_y & 0 \\ 0 & 0 & \varepsilon_z \end{bmatrix}, \tag{1}$$

where material parameters $\varepsilon_x$, $\varepsilon_y$ and $\varepsilon_z$ may be complex due to the intrinsic loss of the material. In principle, in $k_x$-$k_z$ space, both $k_x$ and $k_z$ can be complex for lossy anisotropic materials. However, for simplicity, here we only consider the space with real $k_x$, since in most cases, the electromagnetic (EM) waves impinge the materials from vacuum with real parallel wave vector $k_x$ preserved. Therefore, we can get the following expressions of EFCs for TM-polarized waves in form of Re$[k_z]$ and Im$[k_z]$, respectively.

$$\left(\frac{k_z^{\mathrm{R}}}{k_0}\right)^2 = \frac{1}{2}\left[\varepsilon_x^{\mathrm{R}} - \frac{1}{|\varepsilon_z|^2}(\varepsilon_x^{\mathrm{R}}\varepsilon_z^{\mathrm{R}} + \varepsilon_x^{\mathrm{I}}\varepsilon_z^{\mathrm{I}})\left(\frac{k_x}{k_0}\right)^2 + |\varepsilon_x|\sqrt{1 + \frac{1}{|\varepsilon_z|^2}\left(\frac{k_x}{k_0}\right)^4 - 2\frac{\varepsilon_z^{\mathrm{R}}}{|\varepsilon_z|^2}\left(\frac{k_x}{k_0}\right)^2}\right] \tag{2}$$

$$\left(\frac{k_z^{\mathrm{I}}}{k_0}\right)^2 = \frac{1}{2}\left[-\varepsilon_x^{\mathrm{R}} + \frac{1}{|\varepsilon_z|^2}(\varepsilon_x^{\mathrm{R}}\varepsilon_z^{\mathrm{R}} + \varepsilon_x^{\mathrm{I}}\varepsilon_z^{\mathrm{I}})\left(\frac{k_x}{k_0}\right)^2 + |\varepsilon_x|\sqrt{1 + \frac{1}{|\varepsilon_z|^2}\left(\frac{k_x}{k_0}\right)^4 - 2\frac{\varepsilon_z^{\mathrm{R}}}{|\varepsilon_z|^2}\left(\frac{k_x}{k_0}\right)^2}\right] \tag{3}$$

Considering the special category of lossy anisotropic materials, which possess $\varepsilon_z^{\mathrm{R}} \to 0$ and $\varepsilon_z^{\mathrm{I}} \to \infty$, Eqs. (2)-(3) will be degenerated to

$$\left(\frac{k_z^{\mathrm{R}}}{k_0}\right)^2 = \frac{1}{2}(\varepsilon_x^{\mathrm{R}} + |\varepsilon_x|) \tag{4}$$

and

$$\left(\frac{k_z^{\mathrm{I}}}{k_0}\right)^2 = \frac{1}{2}(-\varepsilon_x^{\mathrm{R}} + |\varepsilon_x|). \tag{5}$$

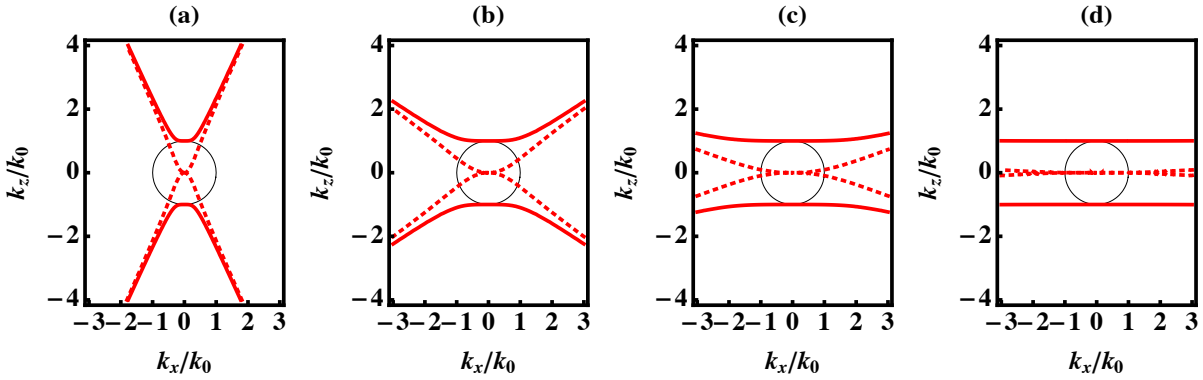


FIG. 1: Equi-frequency contours of $\mathrm{Re}[k_z]/k_0$ (thick solid curve) and $\mathrm{Im}[k_z]/k_0$ (thick dotted curve) with respect to $k_x/k_0$ for lossy anisotropic materials with $\varepsilon_x = 1$ but $\varepsilon_z = 0.1i$ (a), $i$ (b), $5i$ (c) and $50i$ (d), respectively. The circular EFC of vacuum (thin solid curve) is set as a reference in each figure.

Figures 1(a)-(d) show the EFCs of $\mathrm{Re}[k_z]/k_0$ (thick solid curve) and $\mathrm{Im}[k_z]/k_0$ (thick dotted curve) with respect to $k_x/k_0$ for anisotropic materials $\varepsilon_z = 0.1i$, $i$, $5i$ and $50i$ ($\varepsilon_x = 1$ for all cases), respectively, in comparison to the circular EFC of vacuum (thin solid curve). From Fig. 1, we find that, as $\varepsilon_z^{\mathrm{I}}$ increases, EFC of $\mathrm{Re}[k_z]/k_0$ becomes flatter and flatter, and surprisingly on the other hand, $\mathrm{Im}[k_z]$ gradually gets smaller. Therefore, clearly according to Fig. 1, we can expect a low-loss beam collimation effect with such a special category of high-loss anisotropic materials, which to some extent is counterintuitive. In addition, we also find the transmission of energy for TM-polarized waves, which is expressed in the form $T^{\mathrm{TM}} = \mathrm{Re}[S_{2z}]/\mathrm{Re}[S_{2x}] = (\mathrm{Re}[k_{2z}/\varepsilon_{2x}]/\mathrm{Re}[k_{1z}/\varepsilon_1])|t^{\mathrm{TM}}|^2$, can keep over 50% even for 80° angle of incidence at the interface of air and lossy anisotropic ENZ materials. Therefore, the introduction of these anisotropic materials will lead to an omnidirectional high efficiency energy collimation effect, which may be greatly beneficial to the field of energy harvesting and storage. Based on the brief discussions as shown above, a large $\mathrm{Im}[\varepsilon_z]$ is desirable to achieve a satisfying beam collimation effect, and we hope the value of $\mathrm{Im}[\varepsilon_x]$ as small as possible to prevent severe decay of collimated beam inside the anisotropic material.

In the present work, we focus on the exploration of possible configurations to achieve the aforementioned lossy anisotropic ENZ materials. Figure 2 shows the schematic of under investigated metal-dielectric-layered structure and wire medium, in both forms of so-called parallel [(a) and (c)] and perpendicular [(b) and (d)] configurations.

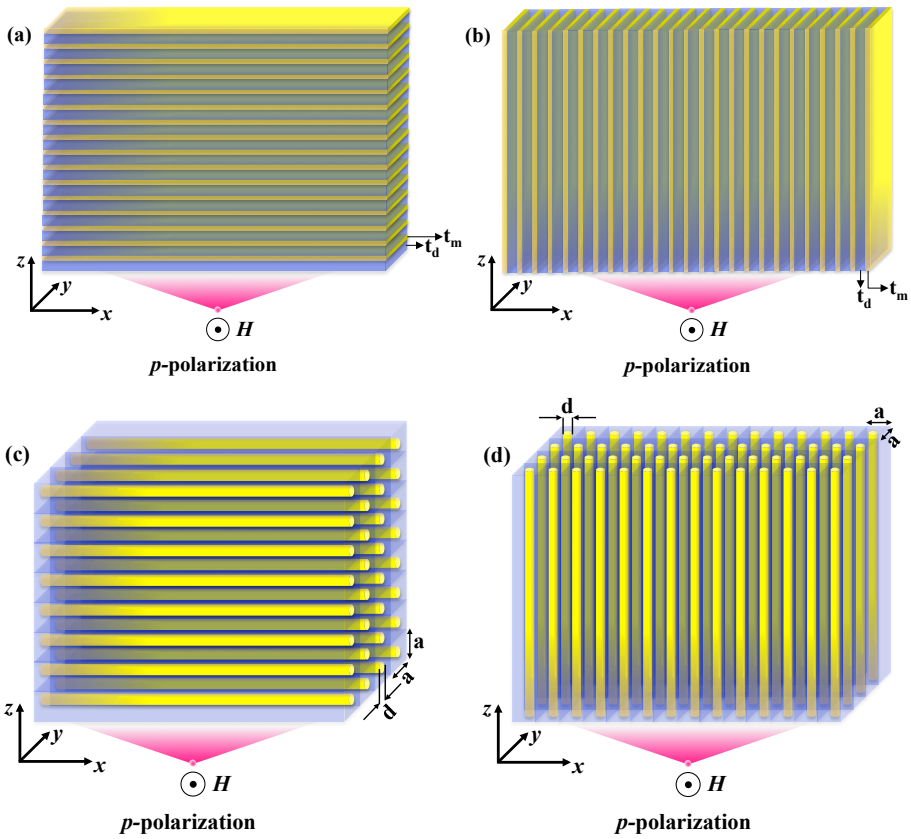


FIG. 2: Schematic of metal-dielectric layered structure [(a)-(b)] and wire medium [(c)-(d)] under parallel [(a) and (c)] and perpendicular [(b) and (d)] configurations, respectively.

### A. Metal-Dielectric-Layered-Stack Structure

For the metal-dielectric-layered structure under parallel configuration as shown in Fig. 1(a), Maxwell-Garnett theory[42] gives

$$\varepsilon_z = \varepsilon_\perp = \frac{1}{f/\varepsilon_{\rm M} + (1-f)/\varepsilon_{\rm D}} \tag{6}$$

and

$$\varepsilon_x = \varepsilon_{//} = f\varepsilon_{\rm M} + (1-f)\varepsilon_{\rm D}, \tag{7}$$

where "$\perp$" ("//") means the direction perpendicular (parallel) to the metal/dielectric layers, $f$ is the filling ratio of metal layers over the period, and $\varepsilon_{\rm M}$ and $\varepsilon_{\rm D}$ represent permittivities of metal and dielectric materials, respectively. For further derivations, $\varepsilon_{\rm M}$ can be written in the form with separated real and imaginary parts as $\varepsilon_{\rm M} = \varepsilon_{\rm M}^{\rm R} + i\varepsilon_{\rm M}^{\rm I}$, so can $\varepsilon_{\rm D} = \varepsilon_{\rm D}^{\rm R} + i\varepsilon_{\rm D}^{\rm I}$. Therefore, from Eq. (6), we can get the expressions of real and imaginary parts of $\varepsilon_z$ as follows

$$\mathrm{Re}[\varepsilon_z] = \frac{f\varepsilon_{\rm M}^{\rm R}|\varepsilon_{\rm D}|^2 + (1-f)\varepsilon_{\rm D}^{\rm R}|\varepsilon_{\rm M}|^2}{f^2|\varepsilon_{\rm D}|^2 + (1-f)^2|\varepsilon_{\rm M}|^2 + 2f(1-f)(\varepsilon_{\rm M}^{\rm R}\varepsilon_{\rm D}^{\rm R} + \varepsilon_{\rm M}^{\rm I}\varepsilon_{\rm D}^{\rm I})}, \tag{8}$$

$$\mathrm{Im}[\varepsilon_z] = \frac{f\varepsilon_{\rm M}^{\rm I}|\varepsilon_{\rm D}|^2 + (1-f)\varepsilon_{\rm D}^{\rm I}|\varepsilon_{\rm M}|^2}{f^2|\varepsilon_{\rm D}|^2 + (1-f)^2|\varepsilon_{\rm M}|^2 + 2f(1-f)(\varepsilon_{\rm M}^{\rm R}\varepsilon_{\rm D}^{\rm R} + \varepsilon_{\rm M}^{\rm I}\varepsilon_{\rm D}^{\rm I})}. \tag{9}$$

To fulfill the condition of $\varepsilon_z = 0$, filling ratio of metal layers needs to have the following value from Eq. (8):

$$f = \frac{\varepsilon_{\rm D}^{\rm R}|\varepsilon_{\rm M}|^2}{\varepsilon_{\rm D}^{\rm R}|\varepsilon_{\rm M}|^2 - \varepsilon_{\rm M}^{\rm R}|\varepsilon_{\rm D}|^2}. \tag{10}$$

By applying Eq. (10) to Eq. (9), we get $\mathrm{Im}[\varepsilon_z]$ in form of material parameters

$$\mathrm{Im}[\varepsilon_z] = \frac{\varepsilon_{\mathrm{D}}^{\mathrm{R}}|\varepsilon_{\mathrm{M}}|^2 - \varepsilon_{\mathrm{M}}^{\mathrm{R}}|\varepsilon_{\mathrm{D}}|^2}{\varepsilon_{\mathrm{D}}^{\mathrm{R}}\varepsilon_{\mathrm{M}}^{\mathrm{I}} - \varepsilon_{\mathrm{M}}^{\mathrm{R}}\varepsilon_{\mathrm{D}}^{\mathrm{I}}}. \tag{11}$$

With respect to $\varepsilon_x$, the real and imaginary parts can be expressed respectively as follows after some algebra derivations:

$$\mathrm{Re}[\varepsilon_x] = \frac{\varepsilon_{\mathrm{D}}^{\mathrm{R}}\varepsilon_{\mathrm{M}}^{\mathrm{R}}(|\varepsilon_{\mathrm{M}}|^2 - |\varepsilon_{\mathrm{D}}|^2)}{\varepsilon_{\mathrm{D}}^{\mathrm{R}}|\varepsilon_{\mathrm{M}}|^2 - \varepsilon_{\mathrm{M}}^{\mathrm{R}}|\varepsilon_{\mathrm{D}}|^2} \tag{12}$$

and

$$\mathrm{Im}[\varepsilon_x] = \frac{\varepsilon_{\mathrm{D}}^{\mathrm{R}}\varepsilon_{\mathrm{M}}^{\mathrm{I}}|\varepsilon_{\mathrm{M}}|^2 - \varepsilon_{\mathrm{M}}^{\mathrm{R}}\varepsilon_{\mathrm{D}}^{\mathrm{I}}|\varepsilon_{\mathrm{D}}|^2}{\varepsilon_{\mathrm{D}}^{\mathrm{R}}|\varepsilon_{\mathrm{M}}|^2 - \varepsilon_{\mathrm{M}}^{\mathrm{R}}|\varepsilon_{\mathrm{D}}|^2}. \tag{13}$$

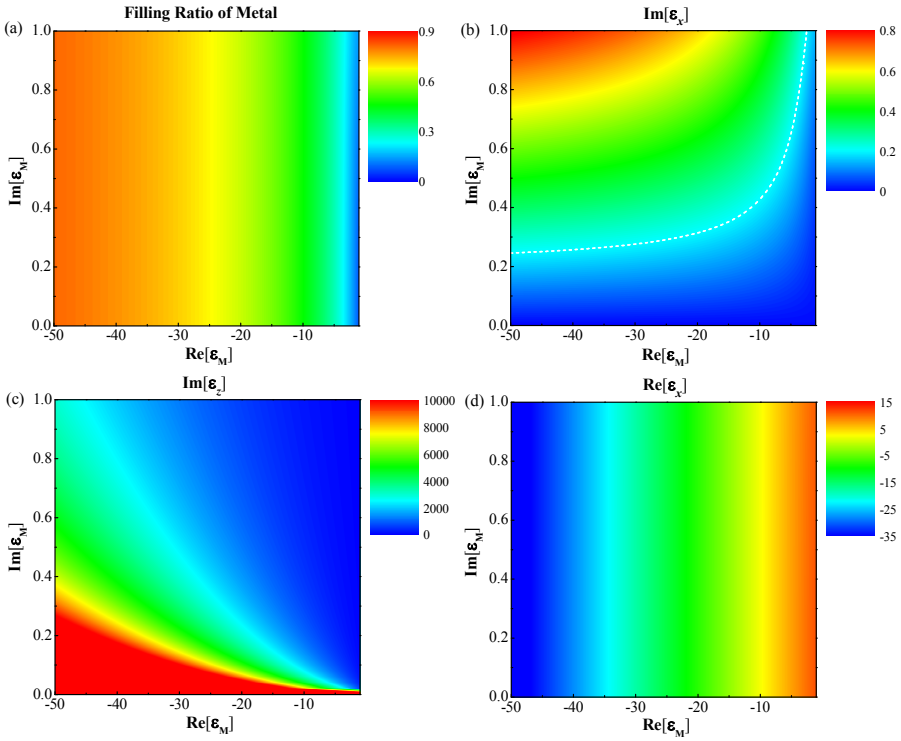


FIG. 3: The case of metal-dielectric-layered structure under configuration I with $\varepsilon_{\mathrm{D}} = 12 + 0.01i$: Dependence of (a) filling ratio of metal for $\mathrm{Re}[\varepsilon_z]$= 0, (b) $\mathrm{Im}[\varepsilon_x]$, (c) $\mathrm{Im}[\varepsilon_z]$ and (d) $\mathrm{Re}[\varepsilon_x]$ with respect to different material parameters of the metal ($\varepsilon_{\mathrm{M}}$). Dashed lines in (b) correspond to $\mathrm{Im}[\varepsilon_x]$= 0.2.

Therefore, with the choice of specific metallic and dielectric materials in the structure of Fig. 2(a), Eqs. (10)-(13) can give us the corresponding value of filling ratio $f$ to construct the lossy anisotropic ENZ material and other material parameters of the effective medium, i.e., $\mathrm{Im}[\varepsilon_z]$, $\mathrm{Re}[\varepsilon_x]$ and $\mathrm{Im}[\varepsilon_x]$. In Fig. 3, we show the results of searching for appropriate metallic materials towards a zero-$\mathrm{Re}[\varepsilon_z]$ anisotropic medium with metal-dielectric-layered structure in the parallel stack configuration [see Fig. 2(a)], for a preset dielectric material with $\varepsilon_{\mathrm{D}} = 12 + 0.01i$. For Figs. 3(a)-(d), $x-$ and $y-$axis correspond to the change of $\mathrm{Re}[\varepsilon_{\mathrm{M}}]$ and $\mathrm{Im}[\varepsilon_{\mathrm{M}}]$, respectively, and the colormap shows the values of targeted parameters. With respect to the filling ratio, we would like it a moderate value to avoid too thin or too thick metal or dielectric layers, and thus Fig.3(a) provides a clear guidance with it. As we already pointed out in the above, the two most important merits for achieving the high-efficiency energy collimation effect are low $\mathrm{Im}[\varepsilon_x]$ and low $\mathrm{Im}[\varepsilon_z]$ of the effective medium, which are indicated in Fig. 3(b) and (c), respectively. The white dashed line in Fig. 3(b) corresponds to the border with $\mathrm{Im}[\varepsilon_x]$=0.2 and we hope the choice of the metallic material can make the value of $\mathrm{Im}[\varepsilon_x]$ settled below it, to prevent dramatic decay of energy inside of the anisotropic medium. On the other hand, according to Fig. 3(c), the metallic materials with parameters sit at bottom left side are desirable to give high $\mathrm{Im}[\varepsilon_z]$. We see $\mathrm{Im}[\varepsilon_x]$ and $\mathrm{Im}[\varepsilon_z]$ do have some contradictory tendency upon the change of property of the

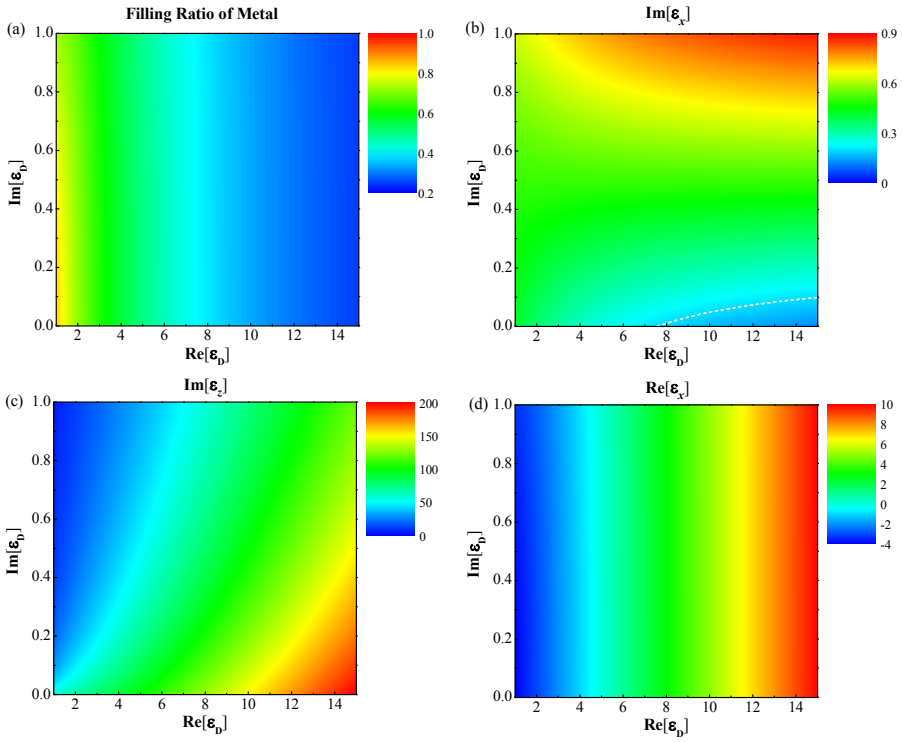


FIG. 4: The case of metal-dielectric-layered structure under configuration I with $\varepsilon_{\rm M} = -5 + 0.5i$: Dependence of (a) filling ratio of metal for Re[$\varepsilon_z$]= 0, (b) Im[$\varepsilon_x$], (c) Im[$\varepsilon_z$] and (d) Re[$\varepsilon_x$] with respect to different material parameters of the dielectric ($\varepsilon_{\rm D}$). Dashed lines in (b) correspond to Im[$\varepsilon_x$]= 0.2.

metallic material, and therefore, we need to compromise these conditions to make the choices of the metallic material accordingly. For a complete impression to the constructed effective medium, the parametric map of Re[$\varepsilon_x$] is shown in Fig. 3(d) for different metallic materials applied in the configuration.

In parallel, Fig. 4 gives the results of searching for appropriate dielectric materials to construct the desired zero-Re[$\varepsilon_z$] anisotropic medium with the configuration of Fig. 2(a), assuming the metallic material has $\varepsilon_{\rm M} = -5 + 0.5i$. From Fig. 4(b), it is required for us to set the $\varepsilon_{\rm D}$ in the area of bottom right corner to get low Im[$\varepsilon_x$] and Fig. 4(c) indicates high Im[$\varepsilon_z$] happens more or less the same area, i.e., a low-loss high-index dielectric material is highly desired in this case. However, on the other hand, we still need to take the filling ratio [see Fig. 4(a)] into account, not to make the condition of potential fabrication too challenging. The colormap of Re[$\varepsilon_x$] is again presented in Fig. 4(d) for a complete knowledge to the constructed layered structure.

As we have seen, our theoretical analysis and numerical calculations do offer us a clear guidance in selecting appropriate ingredients to construct a satisfying high-loss anisotropic ENZ medium with the metal-dielectric-layered configuration in Fig. 2(a). By searching various plasmonic materials accordingly, we find aluminum-doped zinc oxide (AZO), which has $\varepsilon_{\rm M} \approx -2 + 0.5i$ at free space wavelength $\lambda = 1.5$ $\mu$m,[43,44] is a good candidate to serve for the metal layers here. With the dielectric $\varepsilon_{\rm D} = 12 + 0.01i$, we would like to perform numerical simulations to the corresponding constructed metal-dielectric layered structure and to its effective medium equivalence as well. Considering the chosen materials, the condition of zero-Re[$\varepsilon_z$] gives the filling ratio $f = 0.15$ and the thicknesses of metallic ($t_{\rm m}$) and dielectric ($t_{\rm d}$) layers are set 15 and 85 nm, respectively. The corresponding $\lambda/t$, where $t = t_{\rm m} + t_{\rm d}$ is the period of the layered structure, will be 15 and the structure thus can be well treated as an effective medium with properties described in Eqs. (6)-(7). Figure 5 shows the effect of energy collimation by setting a magnetic line source in vacuum in front of the designed metal-dielectric-layered structure of (b) and its effective medium equivalence (a). The simulations are performed with the commercial software COMSOL Multiphysics with perfectly matched layers assigned at all the surrounding boundaries. According to Fig. 5, the beams of almost any angle of incidence are collimated inside of such an anisotropic medium with fairly low decay in the propagation. The perfect consistency in results for realistic stacked structure and corresponding effective medium, is also an indication that the layered configuration considered here can be very well treated as an effective medium.

Similarly, we can also study the possibilities of realizing the high-loss zero-Re[$\varepsilon_z$] anisotropic medium with the other configuration of metal-dielectric-layered structure shown in Fig. 2(b). According to Maxwell-Garnett theory,[42] we

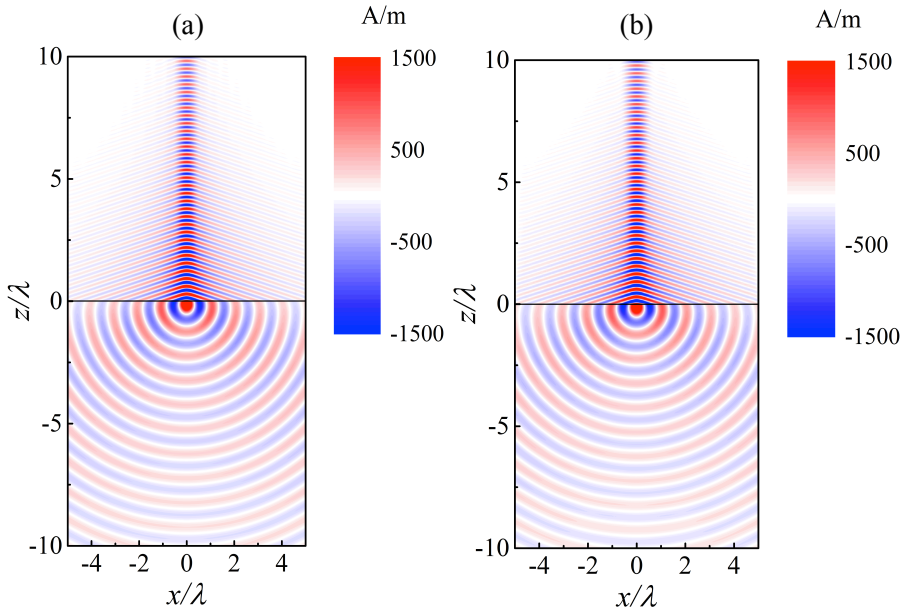


FIG. 5: $y$-component of magnetic field, i.e., $H_y$ for metal-dielectric-layered structure at $\lambda = 1.5\mu$m under configuration I: (a) Homogeneous effective medium equivalence and (b) realistic layered structure. Metal layers are 15 nm-thick AZO with $\varepsilon_{\rm M} = -2 + 0.5i$ and dielectric layers have $\varepsilon_{\rm D} = 12 + 0.01i$ with the thickness of 85 nm.

get

$$\varepsilon_z = \varepsilon_{//} = f\varepsilon_{\rm M} + (1-f)\varepsilon_{\rm D}, \tag{14}$$

and

$$\varepsilon_x = \varepsilon_{\perp} = \frac{1}{f/\varepsilon_{\rm M} + (1-f)/\varepsilon_{\rm D}}. \tag{15}$$

By setting Re[$\varepsilon_z$]=0, we can easily get the simple expression of the required filling ratio of metallic layers in form of $\varepsilon_{\rm M}$ and $\varepsilon_{\rm D}$ as following

$$f = \frac{\varepsilon_{\rm D}^{\rm R}}{\varepsilon_{\rm D}^{\rm R} - \varepsilon_{\rm M}^{\rm R}}. \tag{16}$$

Then, Im[$\varepsilon_z$] can also be expressed in a simple form as

$$\mathrm{Im}[\varepsilon_z] = \frac{\varepsilon_{\rm D}^{\rm R}\varepsilon_{\rm M}^{\rm I} - \varepsilon_{\rm M}^{\rm R}\varepsilon_{\rm D}^{\rm I}}{\varepsilon_{\rm D}^{\rm R} - \varepsilon_{\rm M}^{\rm R}}. \tag{17}$$

For $\varepsilon_x$, we can also replace $f$ with Eq. (16) in Eq. (15), and extract Im[$\varepsilon_x$]. It is found the expression of parametric dependence of Im[$\varepsilon_x$] is fairly complicated, so the relevant information may be understood more intuitively through the direct numerical calculations, which will be shown below.

Figures 6(a)-(d) present the dependence of filling ratio of metallic layers $f$ for Re[$\varepsilon_z$]=0, Im[$\varepsilon_x$], Im[$\varepsilon_z$] and Re[$\varepsilon_x$], respectively, on the property of the metallic material in the configuration of Fig. 2(b), for a preset dielectric material $\varepsilon_{\rm D} = 12 + 0.01i$. From Figs. 6(b) and (c), we can see we should choose a metallic material with both large Re[$\varepsilon_{\rm M}$] and Im[$\varepsilon_{\rm M}$] to achieve the conditions of low Im[$\varepsilon_x$] and high Im[$\varepsilon_z$] for a satisfying high-efficiency energy collimation effect. In contrast, we show, in Fig. 7, the results for the configuration in Fig. 2(b) with $\varepsilon_{\rm M}$ pre-assumably to be $-100 + 100i$ but playing with different dielectric materials. The white dashed line in Fig. 7(b), which corresponds to Im[$\varepsilon_x$] = 0.2, defines the desired area for the choice of the dielectric material for low decay of collimated beam inside

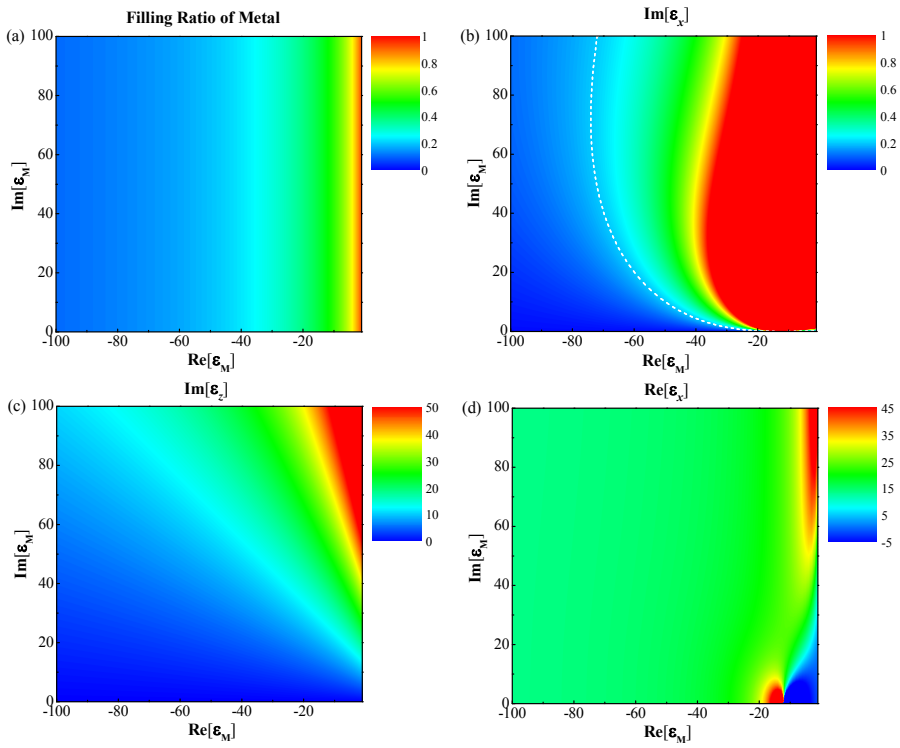


FIG. 6: The case of metal-dielectric-layered structure under configuration II with $\varepsilon_{\rm D} = 12 + 0.01i$: Dependence of (a) filling ratio of metal for Re[$\varepsilon_z$]= 0, (b) Im[$\varepsilon_x$], (c) Im[$\varepsilon_z$] and (d) Re[$\varepsilon_x$] with respect to different material parameters of the metal ($\varepsilon_{\rm M}$). Dashed lines in (b) correspond to Im[$\varepsilon_x$]= 0.2.

of the anisotropic medium. With also $f$ and Im[$\varepsilon_z$] are taken into account, we conclude that the bottom area is still preferred.

Indeed, Figs. 6-7 clearly guide us in searching for proper ingredient especially the metallic material to build the desired anisotropic medium under the configuration in Fig. 2(b), and accordingly, we find Zirconium Nitride (ZrN) with $\varepsilon_{\rm M} = -172.73 + 196.92i$ at $\lambda = 3$ $\mu$m[44] should be a good choice for metal layers here. We therefore consider an example construction of Fig. 2(b) made by ZrN and a dielectric material with $\varepsilon_{\rm D} = 10 + 0.001i$ to demonstrate the desired energy collimation effect by performing corresponding full-wave simulations. The thicknesses of ZrN and dielectric layers are 16.5 and 283.5 nm, respectively, and $\lambda/t \sim 10$ makes the effective medium equivalence still hold. Figure 8 shows the simulation results of $y$-component of the magnetic field ($H_y$) for a magnetic line source placed in the vacuum in front of the designed anisotropic medium for both realistic metal-dielectric-layered structure [Fig. 8(b)] and its effective medium equivalence [Fig. 8(a)], respectively. We again demonstrate the decent energy collimation for our design, which suffers from some broadening effect along the propagation inside the anisotropic medium compared to the previous parallel-stack configuration. The effective medium theory is also proved to work perfectly here by comparing Figs. 8(a) and (b), which show almost the same field distribution in both cases. Therefore, such a configuration can serve as a candidate for a practical device of energy collimation as well.

### B. Wire Medium Structure

Wire medium, specifically corresponding to metallic wires embedded in the matrix of some dielectric material here, is another popular metamaterial structure, which has been extensively studied in the past decades, both in theory and experiment.[45–48] It may also be described with the effective medium theory with the properties mathematically predicted in form of $\varepsilon_{\rm M}$, $\varepsilon_{\rm D}$ and the filling ratio of metallic wires $f$. To construct the expected lossy zero-Re[$\varepsilon_z$] anisotropic medium with wire medium, both the so-called parallel and perpendicular configurations as shown in Figs. 2(c) and (d), respectively, are considered and discussed in the following.

Firstly, we would like to investigate the parallel configuration, the effective medium parameters of which can be expressed as[42]

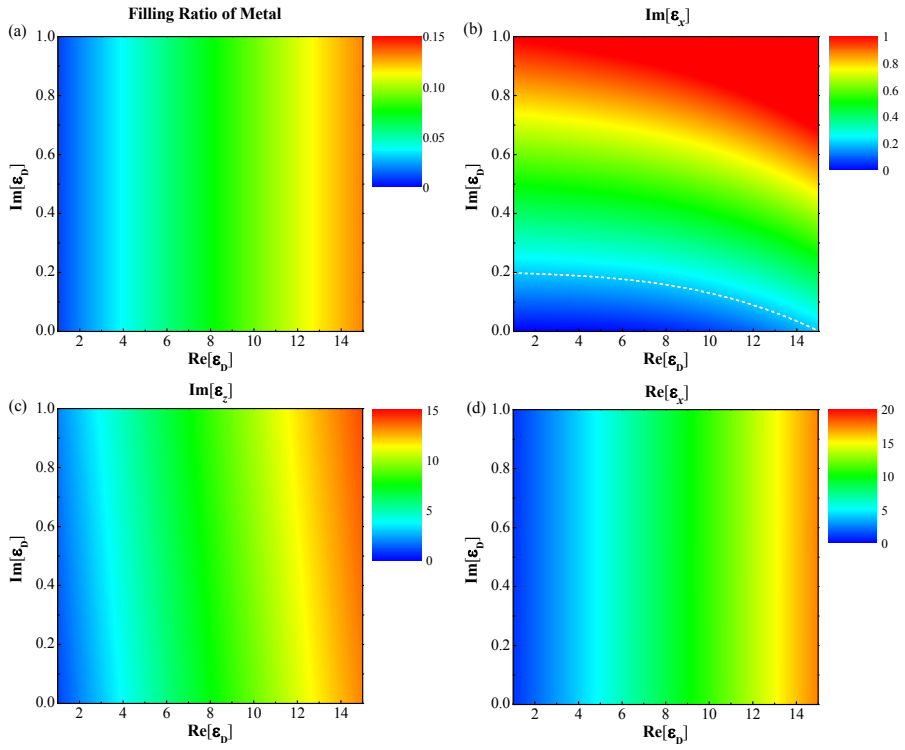


FIG. 7: The case of metal-dielectric-layered structure under configuration II with $\varepsilon_{\rm M} = -100 + 100i$: Dependence of (a) filling ratio of metal for Re[$\varepsilon_z$]= 0, (b) Im[$\varepsilon_x$], (c) Im[$\varepsilon_z$] and (d) Re[$\varepsilon_x$] with respect to different material parameters of the dielectric ($\varepsilon_{\rm D}$). Dashed lines in (b) correspond to Im[$\varepsilon_x$]= 0.2.

$$\varepsilon_z = \varepsilon_\perp = \varepsilon_{\rm D}\frac{(1+f)\varepsilon_{\rm M} + (1-f)\varepsilon_{\rm D}}{(1-f)\varepsilon_{\rm M} + (1+f)\varepsilon_{\rm D}}, \tag{18}$$

and

$$\varepsilon_x = \varepsilon_{//} = f\varepsilon_{\rm M} + (1-f)\varepsilon_{\rm D}. \tag{19}$$

Since the condition of zero-Re[$\varepsilon_z$] will lead to a fairly complicated form of $f$ and the following $\varepsilon_{x,z}$ as well, which are not intuitive, we would like to numerically search appropriate materials to construct the desired wire medium, instead of presenting the analytical expressions.

Figure 9 shows the dependence of $f$, Im[$\varepsilon_z$], Im[$\varepsilon_x$] and Re[$\varepsilon_x$] on the properties of metallic wires for a pre-set dielectric matrix material, which has $\varepsilon_{\rm D} = 12 + 0.01i$. The metallic material with $\varepsilon_{\rm M}$ settled within the area of white dashed line (corresponding to Im[$\varepsilon_x$] = 0.2) in Fig. 9(b) is preferred, for relatively lower loss of the collimated EM waves in propagation in the constructed anisotropic medium. Fig. 9(c) provides the guidance for the choice of metallic material leading to a better collimation effect of energy with larger Im[$\varepsilon_z$], and we find left bottom area of $\varepsilon_{\rm M}$ is more desirable. On the other hand, a moderate value for the filling ratio of metallic wires needs to be taken into account as well, as shown in Fig. 9(a). We should be noted that $\varepsilon_{\rm M}$ of practical metallic materials may also compromise and limit our choices and the corresponding collimation effect of the wire medium.

In contrast, we also numerically studied the wire medium in the parallel-stack configuration [shown in Fig. 2(c)] by setting $\varepsilon_{\rm M} = -5 + 0.5i$ but playing with $\varepsilon_{\rm D}$, and the results are presented in Fig. 10, which provides us a clear guidance for the choice of appropriate dielectric matrix material by compromising the requirements of small Im[$\varepsilon_x$] [below 0.2 within the white dashed line area in Fig. 10(b)], large Im[$\varepsilon_z$] [left bottom corner area in Fig. 10(c)] and moderate value of filling ratio $f$ [see Fig. 10(a)].

Indicated by the numerical results in Figs. 9 and 10, we choose AZO ($\varepsilon_{\rm M} \approx -2 + 0.5i$ at around $\lambda = 1.5$ $\mu$m[43,44]) for the wires, which are embedded in a dielectric matrix with $\varepsilon_{\rm D} = 2 + 0.01i$ in the format of parallel stack. From Eqs. 18 and 19, we set the radius of AZO wires to be 20 nm and the lattice constant $a = 100$ nm, so $\lambda/a$ reaches 15.

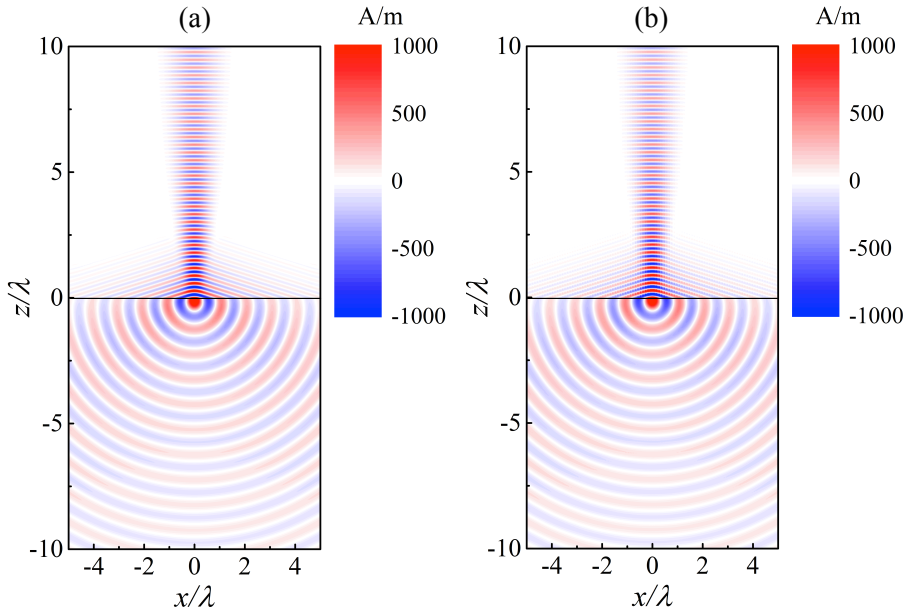


FIG. 8: $y$-component of magnetic field, i.e., $H_y$ for metal-dielectric-layered structure at $\lambda = 3$ $\mu$m (frequency 100 THz) under configuration II: (a) Homogeneous effective medium equivalence and (b) realistic layered structure. Metal layers are 16.5 nm-thick ZrN with $\varepsilon_{\rm M} = -172.73 + 196.92i$ and dielectric layers are 283.5 nm-thick with $\varepsilon_{\rm D} = 10 + 0.001i$.

The calculated $\varepsilon_z \approx 4.7 \times 10^{-3} + 2.26i$ and $\varepsilon_x \approx 1.50 + 0.07i$. We show the results of our full-wave simulations to the designed wire medium and its effective medium equivalence in Figs. 11 (b) and (a), respectively. The similar effect of beam collimation is demonstrated for both cases. The beam propagates with fairly low decay inside of the anisotropic medium due to the small value of Im$[\varepsilon_x]$. On the other hand, small Im$[\varepsilon_z]$ of only 2.26 leads to the broadening tendency of the collimated beam in the propagation.

Finally, we would like to discuss the possibility of realizing the lossy zero-Re$[\varepsilon_z]$ anisotropic material with the so-called perpendicular configuration of wire medium, as shown in Fig. 2(d). In the scope of effective medium, $\varepsilon_x$ and $\varepsilon_z$ of the wire medium will have the following forms[42]

$$\varepsilon_z = \varepsilon_{//} = f\varepsilon_{\rm M} + (1-f)\varepsilon_{\rm D} \tag{20}$$

and

$$\varepsilon_x = \varepsilon_{\perp} = \varepsilon_{\rm D}\frac{(1+f)\varepsilon_{\rm M} + (1-f)\varepsilon_{\rm D}}{(1-f)\varepsilon_{\rm M} + (1+f)\varepsilon_{\rm D}}. \tag{21}$$

From Eq. (21), the condition of zero-Re$[\varepsilon_z]$ can give us the required filling ratio of wires $f$:

$$f = \frac{\varepsilon_{\rm D}^{\rm R}}{\varepsilon_{\rm D}^{\rm R} - \varepsilon_{\rm M}^{\rm R}}. \tag{22}$$

With Eqs. (21) and (23), we will easily get the expression of Im$[\varepsilon_z]$ in form of $\varepsilon_{\rm M}$ and $\varepsilon_{\rm D}$

$$\mathrm{Im}[\varepsilon_z] = \frac{\varepsilon_{\rm D}^{\rm R}\varepsilon_{\rm M}^{\rm I} - \varepsilon_{\rm M}^{\rm R}\varepsilon_{\rm D}^{\rm I}}{\varepsilon_{\rm D}^{\rm R} - \varepsilon_{\rm M}^{\rm R}}. \tag{23}$$

Due to the complexity of Eq. (21), there will be no simple expressions of Im$[\varepsilon_x]$ or Re$[\varepsilon_x]$. Therefore, the same as the other configuration of wire medium, it will be more intuitive and straightforward to numerically investigate the dependence of Im$[\varepsilon_x]$ and Re$[\varepsilon_x]$ on the properties of metallic wires $\varepsilon_{\rm M}$ and dielectric matrix material $\varepsilon_{\rm D}$, so as $f$ and Im$[\varepsilon_z]$. Then, we can choose appropriate materials to construct the wire medium accordingly. Two sets of numerical

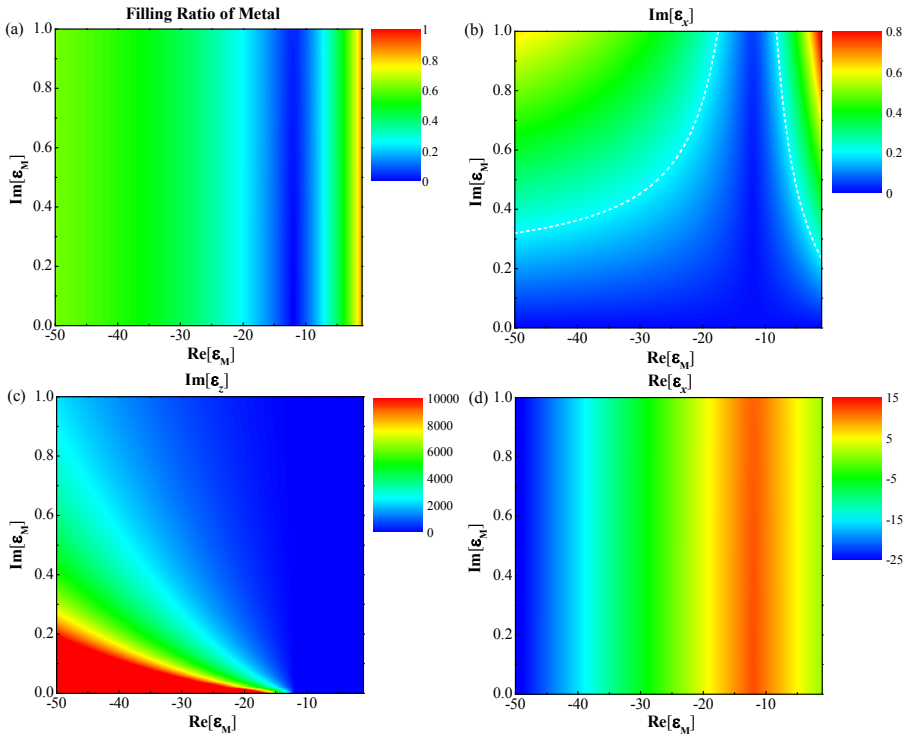


FIG. 9: The case of wire medium under configuration I with $\varepsilon_{\rm D} = 12 + 0.01i$: Dependence of (a) filling ratio of metal for $\mathrm{Re}[\varepsilon_z]= 0$, (b) $\mathrm{Im}[\varepsilon_x]$, (c) $\mathrm{Im}[\varepsilon_z]$ and (d) $\mathrm{Re}[\varepsilon_x]$ with respect to different material parameters of the metal ($\varepsilon_{\rm M}$). Dashed lines in (b) correspond to $\mathrm{Im}[\varepsilon_x]= 0.2$.

results are presented in Figs. 12 and 13, which correspond to the cases of different $\varepsilon_{\rm M}$ with a preset $\varepsilon_{\rm D} = 5 + 0.01i$ (Fig. 12) and different $\varepsilon_{\rm D}$ with a fixed $\varepsilon_{\rm M} = -100 + 100i$ for a hypothetic metallic material (Fig. 13), respectively. In both figures, the dashed line again separates the areas of $\mathrm{Im}[\varepsilon_z] < 0.2$ and $\mathrm{Im}[\varepsilon_z] > 0.2$, so we can firstly set the preferred regime of the materials to avoid any severe decay of the collimated beam inside of the wire medium. According to Fig. 12(c) or Fig. 13(c), we clear see the tendency in the change of $\mathrm{Im}[\varepsilon_z]$ for different $\varepsilon_{\rm M}$ or $\varepsilon_{\rm D}$, and therefore, we know what materials we are pursuing for large $\mathrm{Im}[\varepsilon_z]$ necessary for a satisfying collimation effect. The same as the discussions to all the other cases in the above, we also need to take into account the corresponding filling ratio $f$, which needs not to make the potential experiments too challenging. All these requirements have to be considered simultaneously to get some compromised choice for materials to construct the expected wire medium.

According to Figs. 12 and 13, ZrN, which has $\varepsilon_{\rm M} \approx -172.73 + 196.92i$ at $\lambda = 3\ \mu$m[44], is again a good option for the metallic wires perpendicularly embedded in the dielectric matrix with $\varepsilon_{\rm D}$ set to be $6 + 0.001i$. The lattice constant is 200 nm with the corresponding $\lambda/a = 15$. From Eq. 23, we get the required radius of the ZrN wires about 20.7 nm. The calculated $\varepsilon_z \approx -0.01 + 6.63i$ and $\varepsilon_x \approx 6.43 + 0.02i$ from Eqs. (20) and (21). The corresponding full-wave simulation results, i.e., distribution of $y$-component of magnetic field for a magnetic line source in the vacuum shining the anisotropic medium, can be found in Fig. 14 with both homogeneous effective medium (a) and realistic wire medium (b) applied, respectively. As expected, the designed wire medium again gets the incident beams beautifully collimated with fairly low decay in propagation.

So far, we have systematically explored the realization of high-loss ENZ anisotropic medium with both the layered structure and wire medium. Through the full-wave simulations, we successfully demonstrated loss-induced transmission enhancement at the interface of ENZ anisotropic medium and the effect of energy collimation for each properly designed configuration. Considering the beam collimation effect associated with EFCs as shown in Fig. 1(d), we need to point out it is not necessarily to strictly have zero $\mathrm{Re}[\varepsilon_z]$ if $|\varepsilon_z|$ can be very large according to Eqs. (2)-(3). Practically, in the presented configurations of high-loss anisotropic ENZ medium, $|\varepsilon_z|$ has a finite value in general and non-zero $\mathrm{Re}[\varepsilon_z]$ may lead to the distortion of the flat EFCs, which hurts the expected energy collimation effect. However, the allowed moderate relaxation to the requirement of zero $\mathrm{Re}[\varepsilon_z]$ provides some flexibility in the recipe of constructing anisotropic medium, and on the other hand, for a designed metamaterial structure, the energy collimation effect may survive within some range of frequencies, which will be greatly beneficial for practical applications.

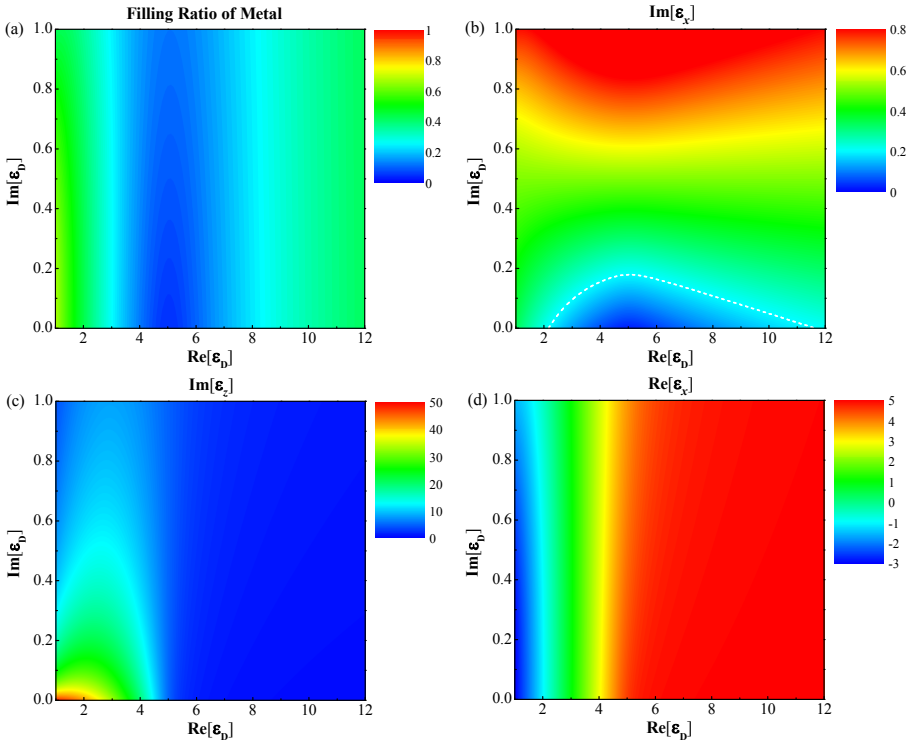


FIG. 10: The case of wire medium under configuration I with $\varepsilon_{\rm M} = -5 + 0.5i$: Dependence of (a) filling ratio of metal for Re[$\varepsilon_z$]= 0, (b) Im[$\varepsilon_x$], (c) Im[$\varepsilon_z$] and (d) Re[$\varepsilon_x$] with respect to different material parameters of the dielectric ($\varepsilon_{\rm D}$). Dashed lines in (b) correspond to Im[$\varepsilon_x$]= 0.2.

## III. CONCLUSIONS

In conclusion, in the scope of effective medium theory, we pursued the possibilities of using metamaterials to realize the special category lossy zero-Re[$\varepsilon_z$] anisotropic medium, which shows a counterintuitive effect of energy collimation. We systematically investigated two simplest metamaterial structures of metal-dielectric-layered stack and wire medium, under both parallel and perpendicular configurations, and provided the corresponding recipes of constructing the proposed lossy zero-Re[$\varepsilon_z$] anisotropic medium via analytical derivations and numerical simulations. As examples, we designed the metamaterial structure with practical ingredient materials for each configuration, and performed full-wave simulations correspondingly to them as well as to their effective medium equivalences. We demonstrated beautiful energy collimation effect for all the example cases and the results are in excellent consistency for the realistic metamaterial and effective medium. Therefore, our current work provides a clear guidance for searching proper metamaterial designs of lossy zero-Re[$\varepsilon_z$] anisotropic medium and thus paves the way towards energy harvesting and wavefront manipulation under such a fabulous strategy.

## IV. ACKNOWLEDGEMENT

Work at Ames Laboratory was partially supported by the U.S. Department of Energy, Office of Basic Energy Science, Division of Materials Sciences and Engineering (Ames Laboratory is operated for the U.S. Department of Energy by Iowa State University under Contract No. DE-AC02-07CH11358), by the U.S. Office of Naval Research, award No. N00014-16-1-2294 (simulations). The European Research Council under the ERC Advanced Grant No. 320081 (PHOTOMETA) supported work (theory) at FORTH.

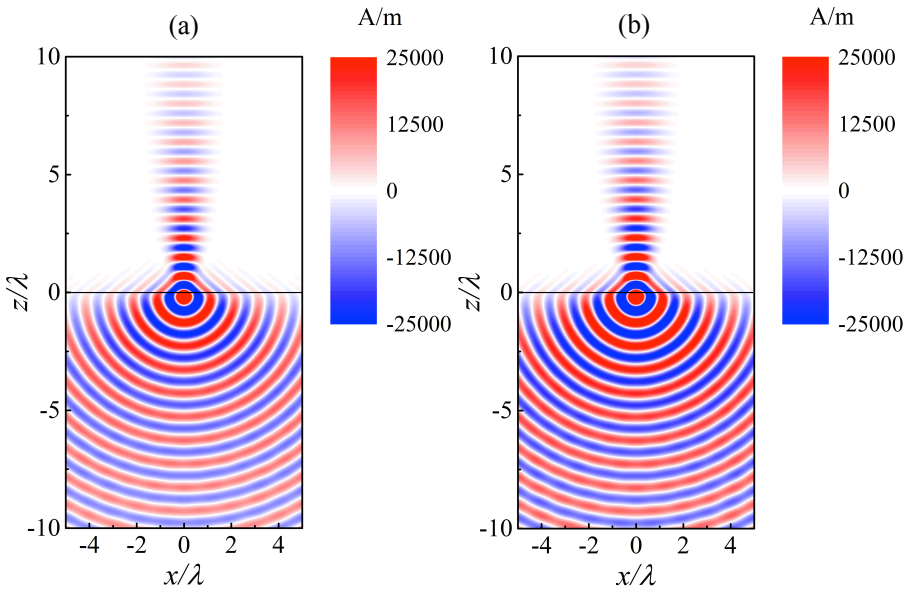


FIG. 11: $y$-component of magnetic field, i.e., $H_y$ for wire medium at $\lambda = 1.5$ $\mu$m (frequency 200 THz) under configuration I: (a) Homogeneous effective medium equivalence and (b) realistic layered structure. Metal wires are 20 nm-radius AZO with $\varepsilon_{\rm M} = -2 + 0.5i$ embedded in dielectric with $\varepsilon_{\rm D} = 2 + 0.01i$ and lattice constant 100 nm.

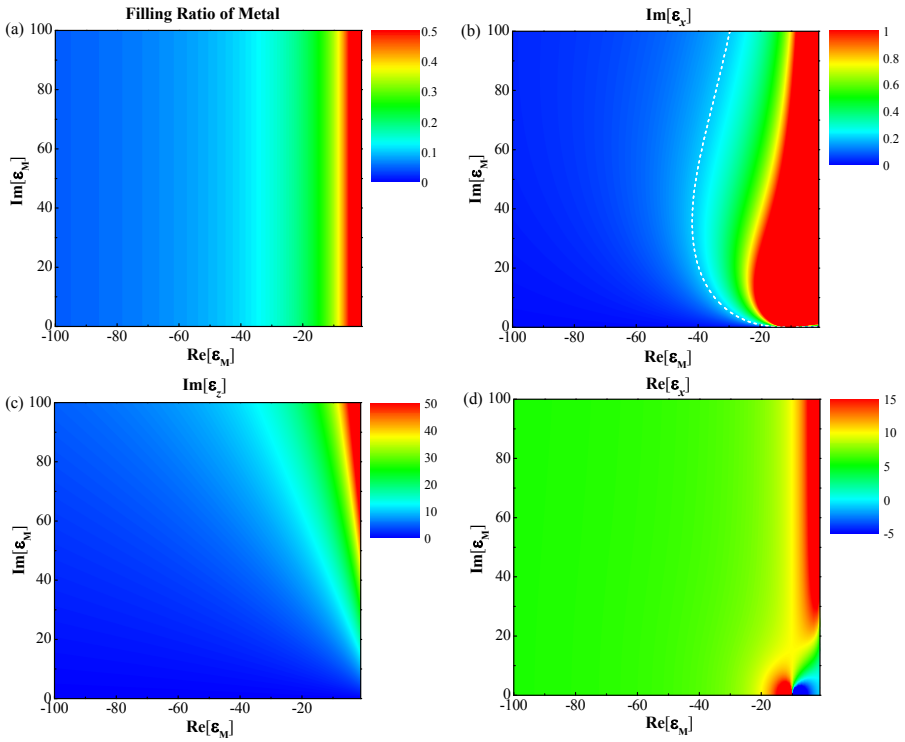


FIG. 12: The case of wire medium under configuration II with $\varepsilon_{\rm D} = 5 + 0.01i$: Dependence of (a) filling ratio of metal for Re[$\varepsilon_z$]= 0, (b) Im[$\varepsilon_x$], (c) Im[$\varepsilon_z$] and (d) Re[$\varepsilon_x$] with respect to different material parameters of the metal ($\varepsilon_{\rm M}$). Dashed lines in (b) correspond to Im[$\varepsilon_x$]= 0.2.

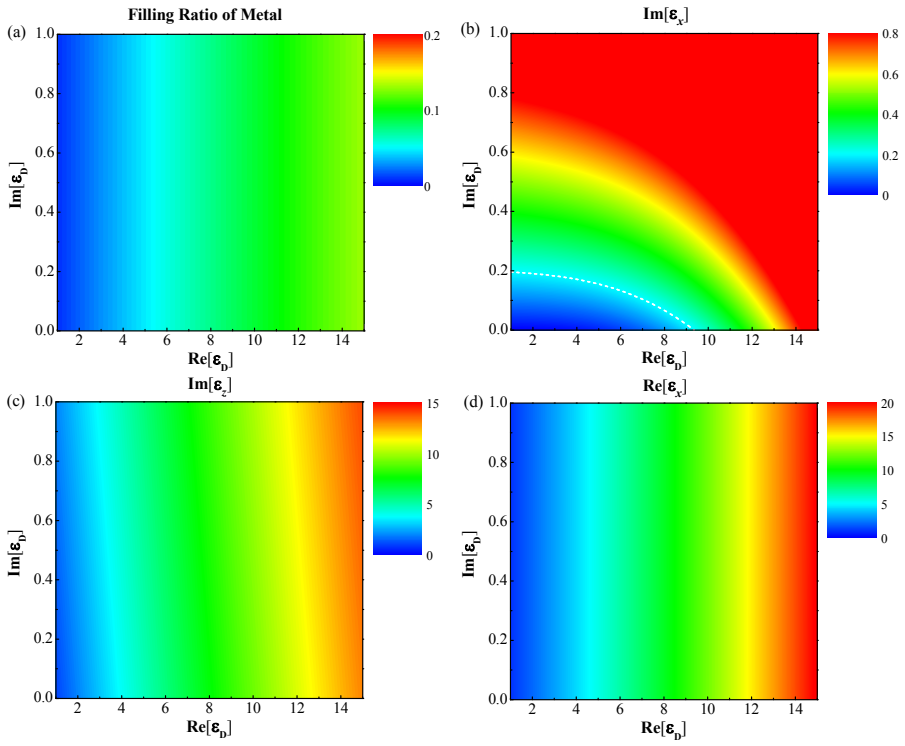


FIG. 13: The case of wire medium under configuration I with $\varepsilon_{\rm M} = -100 + 100i$: Dependence of (a) filling ratio of metal for $\mathrm{Re}[\varepsilon_z]= 0$, (b) $\mathrm{Im}[\varepsilon_x]$, (c) $\mathrm{Im}[\varepsilon_z]$ and (d) $\mathrm{Re}[\varepsilon_x]$ with respect to different material parameters of the dielectric ($\varepsilon_{\rm D}$). Dashed lines in (b) correspond to $\mathrm{Im}[\varepsilon_x]= 0.2$.

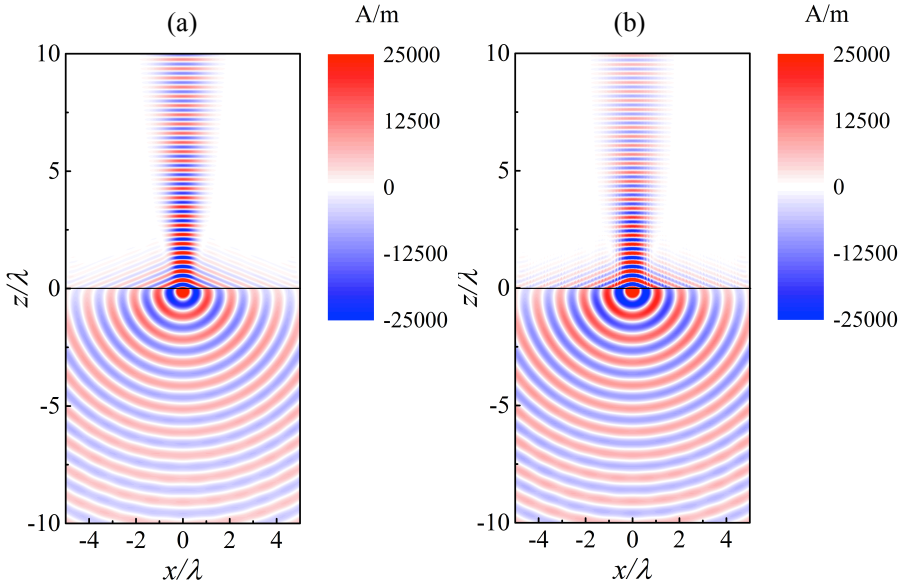


FIG. 14: $y$-component of magnetic field, i.e., $H_y$ for wire medium at $\lambda = 3$ $\mu$m (frequency 100 THz) under configuration II: (a) Homogeneous effective medium equivalence and (b) realistic layered structure. Metal wires are 20.7 nm-radius ZrN with $\varepsilon_{\rm M} = -172.73 + 196.92i$ embedded in dielectric with $\varepsilon_{\rm D} = 6 + 0.001i$ and lattice constant 200 nm.

* nhshen@ameslab.gov


[1] C. M. Soukoulis and M. Wegener, Nature Photon. **5**, 523 (2011).
[2] N. I. Zheludev and Y. S. Kivshar, Nature Mater. **11**, 917 (2012).
[3] H. Chen, C. T. Chen, and P. Sheng, Nature Mater. **9**, 387 (2010).
[4] Y. Liu and X. Zhang, Chem. Soc. Rev. **40**, 2494 (2011).
[5] R. A. Shelby, D. R. Smith, and S. Schultz, Science **292**, 77 (2001).
[6] J. Valentine, S. Zhang, Th. Zentgraf, E. Ulin-Avila, D. A. Genov, G. Bartal, and X. Zhang, Nature **455**, 376 (2008).
[7] J. B. Pendry, Phys. Rev. Lett. **85**, 3966 (2000).
[8] N. Fang, H. Lee, C. Sun, and X. Zhang, Science **308**, 534 (2005).
[9] Z. Liu, H. Lee, Y. Xiong, C. Sun, and X. Zhang, Science **315**, 1686 (2007).
[10] D. Lu and Z. Liu, Nature Commun. **3**, 1205 (2012).
[11] J. B. Pendry, D. Schurig, and D. R. Smith, Science **312**, 1780 (2006).
[12] D. Schurig, J. J. Mock, B. J. Justice, S. A. Cummer, A. F. Starr, and D. R. Smith, Science **314**, 977 (2006).
[13] L. H. Gabrielli, J. Cardenas, C. B. Poitras, and M. Lipson, Nature Photon. **3**, 461 (2009).
[14] J. Valentine, J. Li, Th. Zentgraf, G. Bartal, and X. Zhang, Nature Mater. **8**, 568 (2009).
[15] N. Yu, P. Genevet, M. A. Kats, F. Aieta, J.-P. Tetienne, F. Capasso, and Z. Gaburro, Science **334**, 333 (2011).
[16] A. V. Kildishev, A. Boltasseva, and V. M. Shalaev, Science **339**, 1232009 (2013).
[17] N. Yu and F. Capasso, Nature Mater. **13**, 139 (2014).
[18] R. W. Ziolkowski, Phys. Rev. E **70**, 046608 (2004).
[19] P. Moitra, Y. Yang, Z. Anderson, I. I. Kravchenko, D. P. Briggs, and J. Valtentine, Nature Photon. **7**, 791 (2013).
[20] Y. Li, S. Kita, P. Munoz, O. Reshef, D. I. Vulis, M. Yin, M. Loncar, and E. Mazur, Nature Photon. **9**, 738 (2015).
[21] S. Enoch, G. Tayeb, P. Sabouroux, N. Guerin, and P. Vincent, Phys. Rev. Lett. **89**, 213902 (2002).
[22] Q. Cheng, W. X. Jiang, and T. J. Cui, Phys. Rev. Lett. **108**, 213903 (2012).
[23] M. Silveririnha and N. Engheta, Phys. Rev. Lett. **97**, 157403 (2006).
[24] R. Liu, Q. Cheng, T. Hand, J. J. Mock, T. J. Cui, S. A. Cummer, and D. R. Smith, Phys. Rev. Lett. **100**, 023903 (2008).
[25] V. C. Nguyen, L. Chen, and K. Halterman, Phys. Rev. Lett. **105**, 233908 (2010).
[26] X. Q. Huang, Y. Lai, Z. H. Hang, H. Zheng, and C. T. Chan, Nature Mater. **10**, 582 (2011).
[27] J. Luo, W. X. Lu, Z. H. Hang, H. Y. Chen, B. Hou, Y. Lai, and C. T. Chan, Phys. Rev. Lett. **112**, 073903 (2014).
[28] Q. Zhao, Z. Xiao, F. Zhang, J. Ma, M. Qiao, Y. Meng, C. Lan, B. Li, J. Zhou, P. Zhang, N.-H. Shen, Th. Koschny, and C. M. Soukoulis, Adv. Mater. **27**, 6187 (2015).
[29] C. M. Soukoulis, S. Linden, and M. Wegener, Science **315**, 47 (2007).
[30] A. Fang, Th. Koschny, M. Wegener, and C. M. Soukoulis, Phys. Rev. B **79**, 241104(R) (2009).
[31] S. Xiao, V. P. Drachev, A. V. Kildishev, X. Ni, U. K. Chettiar, H.-K. Yuan, and V. M. Shalaev, Nature Mater. **466**, 735 (2010).
[32] O. Hess, J. B. Pendry, S. A. Maier, R. F. Oulton, J. M. Hamm, and K. L. Tsakmakidis, Nature Mater. **11**, 573 (2012).
[33] N. I. Landy, S. Sajuyigbe, J. J. Mock, D. R. Smith, and W. J. Padilla, Phys. Rev. Lett. **100**, 207402 (2008).
[34] S. Feng, Phys. Rev. Lett. **108**, 193904 (2012).
[35] S. A. Ramakrishna, J. B. Pendry, M. C. K. Wiltshire, and W. J. Stewart, J. Mod. Phys. **50**, 1419 (2002).
[36] P. A. Belov and Y. Hao, Phys. Rev. B **73**, 113110 (2006).
[37] P. A. Belov, Y. Hao, and S. Sudhakaran, Phys. Rev. B **73**, 033108 (2006).
[38] M. G. Silveirinha, P. A. Belov, and C. R. Simovski, Phys. Rev. B **75**, 035108 (2007).
[39] M. G. Silveirinha and N. Engheta, Phys. Rev. B **85**, 085116 (2012).
[40] L. Sun, S. Feng, and X. D. Yang, Appl. Phys. Lett. **101**, 241101 (2012).
[41] H. Jiang, W. Liu, K. Yu, K. Fang, Y. Sun, Y. Li, and H. Chen, Phys. Rev. B **91**, 045302 (2015).
[42] T. C. Choy, *Effective Medium Theory: Principles and Applications* (Oxford University Press, 1999).
[43] G. V. Naik, J. Liu, A. V. Kildishev, V. M. Shalaev, and A. Boltasseva, Proc. Natl. Acad. Sci. USA **109**, 8834 (2012).
[44] G. V. Naik, V. M. Shalaev, and A. Boltasseva, Adv. Mater. **25**, 3264 (2013).
[45] J. Yao, Z. Liu, Y. Liu, Y. Wang, C. Sun, G. Bartal, A. M. Stacy, and X. Zhang, Science **321**, 930 (2008).
[46] Y. Liu, G. Bartal, and X. Zhang, Opt. Express **16**, 15439 (2008).
[47] A. Fang, Th. Koschny, and C. M. Soukoulis, Phys. Rev. B **79**, 245127 (2009).
[48] J. Yao, X. Yang, X. Yin, G. Bartal, and X. Zhang, Proc. Natl. Acad. Sci. USA **108**, 11327 (2011).